Two-axis MEMS Scanning Catheter for Ultrahigh Resolution Three-dimensional and *En Face* Imaging

Aaron D. Aguirre, Paul R. Herz, Yu Chen, James G. Fujimoto

Department of Electrical Engineering and Computer Science and Research Laboratory of Electronics
Massachusetts Institute of Technology, Cambridge, MA 02139, USA
jgfuji@mit.edu

Wibool Piyawattanametha, Li Fan, Ming C. Wu

Department of Electrical Engineering and Computer Science and Integrated Photonics Laboratory,
University of California, Berkeley, CA 94720

Abstract: Ultrahigh resolution two and three-dimensional optical coherence tomography (OCT) imaging was performed using a miniaturized, two-axis scanning catheter based upon microelectromechanical systems (MEMS) mirror technology. The catheter incorporated a custom-designed and fabricated, 1-mm diameter MEMS mirror driven by angular vertical comb (AVC) actuators on both an inner mirror axis and an outer, orthogonal gimbal axis. Using a differential drive scheme, a linearized position response over +/- 6 degrees mechanical angle was achieved. The flexible, fiber-optic catheter device measured < 5 mm in outer diameter with a rigid length of ~ 2.5 cm at the distal end. *In vivo* and *ex vivo* images are presented with < 4 μm axial and ~ 12 μm transverse resolution in tissue.

OCIS codes: (170.4500) Optical coherence tomography; (170.2150) Endoscopic Imaging; (350.3950) Micro-optics; (110.6880) Three-dimensional image acquisition; (120.5800) Scanners

References and links

1. G. J. Tearney, S. A. Boppart, B. E. Bouma, M. E. Brezinski, N. J. Weissman, J. F. Southern, and J. G. Fujimoto, "Scanning single-mode fiber optic catheter-endoscope for optical coherence tomography," Opt. Lett. **21**, 543-545 (1996).
2. G. J. Tearney, M. E. Brezinski, B. E. Bouma, S. A. Boppart, C. Pitris, J. F. Southern, and J. G. Fujimoto, "In vivo endoscopic optical biopsy with optical coherence tomography," Science **276**, 2037-2039 (1997).
3. B. E. Bouma, G. J. Tearney, C. C. Compton, and N. S. Nishioka, "High-resolution imaging of the human esophagus and stomach in vivo using optical coherence tomography," Gastrointest. Endosc. **51**, 467-474 (2000).
4. M. V. Sivak, Jr., K. Kobayashi, J. A. Izatt, A. M. Rollins, R. Ung-Runyawee, A. Chak, R. C. Wong, G. A. Isenberg, and J. Willis, "High-resolution endoscopic imaging of the GI tract using optical coherence tomography," Gastrointest. Endosc. **51**, 474-479 (2000).
5. S. Jackle, N. Gladkova, F. Feldchtein, A. Terentieva, B. Brand, G. Gelikonov, V. Gelikonov, A. Sergeev, A. Fritscher-Ravens, J. Freund, U. Seitz, S. Schroder, and N. Soehendra, "In vivo endoscopic optical coherence tomography of esophagitis, Barrett's esophagus, and adenocarcinoma of the esophagus," Endoscopy **32**, 750-755 (2000).
6. X. D. Li, S. A. Boppart, J. Van Dam, H. Mashimo, M. Mutinga, W. Drexler, M. Klein, C. Pitris, M. L. Krinsky, M. E. Brezinski, and J. G. Fujimoto, "Optical coherence tomography: advanced technology for the endoscopic imaging of Barrett's esophagus," Endoscopy **32**, 921-930 (2000).
7. J. M. Poneros, S. Brand, B. E. Bouma, G. J. Tearney, C. C. Compton, and N. S. Nishioka, "Diagnosis of specialized intestinal metaplasia by optical coherence tomography," Gastroenterology **120**, 7-12 (2001).
8. R. Leitgeb, C. K. Hitzenberger, and A. F. Fercher, "Performance of Fourier domain vs. time domain optical coherence tomography," Opt. Express **11**, 889-894 (2003), http://www.opticsinfobase.org/abstract.cfm?URI=oe-11-8-889.

#77304 - $15.00 USD Received 20 November 2006; revised 12 February 2007; accepted 14 February 2007

9. M. A. Choma, M. V. Sarunic, C. H. Yang, and J. A. Izatt, "Sensitivity advantage of swept source and Fourier domain optical coherence tomography," Opt. Express **11**, 2183-2189 (2003), http://www.opticsinfobase.org/abstract.cfm?URI=oe-11-18-2183.
10. J. F. de Boer, B. Cense, B. H. Park, M. C. Pierce, G. J. Tearney, and B. E. Bouma, "Improved signal-to-noise ratio in spectral-domain compared with time-domain optical coherence tomography," Opt. Lett. **28**, 2067-2069 (2003).
11. S. H. Yun, G. J. Tearney, J. F. de Boer, N. Iftimia, and B. E. Bouma, "High-speed optical frequency-domain imaging," Opt. Express **11**, 2953-2963 (2003), http://www.opticsinfobase.org/abstract.cfm?URI=oe-11-22-2953.
12. N. A. Nassif, B. Cense, B. H. Park, M. C. Pierce, S. H. Yun, B. E. Bouma, G. J. Tearney, T. C. Chen, and J. F. de Boer, "In vivo high-resolution video-rate spectral-domain optical coherence tomography of the human retina and optic nerve," Opt. Express **12**, 367-376 (2004), http://www.opticsinfobase.org/abstract.cfm?URI=oe-12-3-367.
13. R. A. Leitgeb, W. Drexler, A. Unterhuber, B. Hermann, T. Bajraszewski, T. Le, A. Stingl, and A. F. Fercher, "Ultrahigh resolution Fourier domain optical coherence tomography," Opt. Express **12**, 2156-2165 (2004), http://www.opticsinfobase.org/abstract.cfm?URI=oe-12-10-2156.
14. M. A. Choma, K. Hsu, and J. A. Izatt, "Swept source optical coherence tomography using an all-fiber 1300-nm ring laser source," J. Biomed. Opt. **10**, 44009 (2005).
15. M. Wojtkowski, V. Srinivasan, J. G. Fujimoto, T. Ko, J. S. Schuman, A. Kowalczyk, and J. S. Duker, "Three-dimensional retinal imaging with high-speed ultrahigh-resolution optical coherence tomography," Ophthalmology **112**, 1734-1746 (2005).
16. R. Huber, M. Wojtkowski, J. G. Fujimoto, J. Y. Jiang, and A. E. Cable, "Three-dimensional and C-mode OCT imaging with a compact, frequency swept laser source at 1300 nm," Opt. Express **13**, 10523-10538 (2005), http://www.opticsinfobase.org/abstract.cfm?URI=oe-13-26-10523.
17. R. Huber, M. Wojtkowski, and J. G. Fujimoto, "Fourier Domain Mode Locking (FDML): A new laser operating regime and applications for optical coherence tomography," Opt. Express **14**, 3225-3237 (2006), http://www.opticsinfobase.org/abstract.cfm?URI=oe-14-8-3225.
18. A. D. Aguirre, P. Hsiung, T. H. Ko, I. Hartl, and J. G. Fujimoto, "High-resolution optical coherence microscopy for high-speed, in vivo cellular imaging," Opt. Lett. **28**, 2064-2066 (2003).
19. S. A. Boppart, B. E. Bouma, C. Pitris, G. J. Tearney, J. G. Fujimoto, and M. E. Brezinski, "Forward-imaging instruments for optical coherence tomography," Opt. Lett. **22**, 1618-1620 (1997).
20. F. Helmchen, M. S. Fee, D. W. Tank, and W. Denk, "A miniature head-mounted two-photon microscope: High-resolution brain imaging in freely moving animals," Neuron **31**, 903-912 (2001).
21. E. J. Seibel and Q. Y. J. Smithwick, "Unique features of optical scanning, single fiber endoscopy," Lasers Surg. Med. **30**, 177-183 (2002).
22. X. Liu, M. J. Cobb, Y. Chen, M. B. Kimmey, and X. Li, "Rapid-scanning forward-imaging miniature endoscope for real-time optical coherence tomography," Opt. Lett. **29**, 1763-1765 (2004).
23. A. L. Polglase, W. J. McLaren, S. A. Skinner, R. Kiesslich, M. F. Neurath, and P. M. Delaney, "A fluorescence confocal endomicroscope for in vivo microscopy of the upper- and the lower-GI tract," Gastrointest. Endosc. **62**, 686-695 (2005).
24. D. L. Dickensheets and G. S. Kino, "Silicon-micromachined scanning confocal optical microscope," J. Microelectromech. Syst. **7**, 38-47 (1998).
25. M. Sakashita, H. Inoue, H. Kashida, J. Tanaka, J. Y. Cho, H. Satodate, E. Hidaka, T. Yoshida, N. Fukami, Y. Tamegai, A. Shiokawa, and S. Kudo, "Virtual histology of colorectal lesions using laser-scanning confocal microscopy," Endoscopy **35**, 1033-1038 (2003).
26. H. Miyajima, N. Asaoka, T. Isokawa, M. Ogata, Y. Aoki, M. Imai, O. Fujimori, M. Katashiro, and K. Matsumoto, "A MEMS electromagnetic optical scanner for a commercial confocal laser scanning microscope," J. Microelectromech. Syst. **12**, 243-251 (2003).
27. W. Piyawattanametha, P. R. Patterson, G. D. J. Su, H. Toshiyoshi, and M. C. Wu, "A MEMS non-interferometric differential confocal scanning optical microscope," presented at Proceedings of 11th International Conference on Solid State Sensors and Actuators Transducers '01/Eurosensors XV, Munich, Germany, 2001.
28. W. Piyawattanametha, J. T. C. Liu, M. J. Mandella, H. Ra, L. K. Wong, P. Hsiung, T. D. Wang, G. S. Kino, and O. Solgaard, "MEMS Based Dual-axes Confocal Reflectance Handheld Microscope for In Vivo Imaging," presented at IEEE/LEOS International Conference on Optical MEMS, 2006.
29. Y. Pan, H. Xie, and G. K. Fedder, "Endoscopic optical coherence tomography based on a microelectromechanical mirror," Opt. Lett. **26**, 1966-1968 (2001).
30. J. M. Zara, S. Yazdanfar, K. D. Rao, J. A. Izatt, and S. W. Smith, "Electrostatic micromachine scanning mirror for optical coherence tomography," Opt. Lett **28**, 628-630 (2003).
31. A. Jain, A. Kopa, Y. T. Pan, G. K. Fedder, and H. K. Xie, "A two-axis electrothermal micromirror for endoscopic optical coherence tomography," IEEE J. Sel. Top. Quantum Electron **10**, 636-642 (2004).
32. B. Qi, A. P. Himmer, L. M. Gordon, X. D. V. Yang, L. D. Dickensheets, and I. A. Vitkin, "Dynamic focus control in high-speed optical coherence tomography based on a microelectromechanical mirror," Opt. Commun. **232**, 123-128 (2004).

#77304 - $15.00 USD Received 20 November 2006; revised 12 February 2007; accepted 14 February 2007

33. W. Piyawattanametha, L. Fan, S. Hsu, M. Fujino, M. C. Wu, P. R. Herz, A. D. Aguirre, Y. Chen, and J. G. Fujimoto, "Two-dimensional endoscopic MEMS scanner for high resolution optical coherence tomography," presented at Conference on Lasers and Electro-Optics (CLEO), San Francisco, CA, USA, 2004.
34. J. T. W. Yeow, V. X. D. Yang, A. Chahwan, M. L. Gordon, B. Qi, I. A. Vitkin, B. C. Wilson, and A. A. Goldenberg, "Micromachined 2-D scanner for 3-D optical coherence tomography," Sens. Actuators A **117**, 331-340 (2005).
35. W. G. Jung, J. Zhang, L. Wang, P. Wilder-Smith, Z. P. Chen, D. T. McCormick, and N. C. Tien, "Three-dimensional optical coherence tomography employing a 2-axis microelectromechanical scanning mirror," IEEE J. Sel. Top. Quantum Electron. **11**, 806-810 (2005).
36. W. Jung, D. T. McCormick, J. Zhang, L. Wang, N. C. Tien, and Z. P. Chen, "Three-dimensional endoscopic optical coherence tomography by use of a two-axis microelectromechanical scanning mirror," App. Phys. Lett. **88**, 163910 (2006).
37. P. R. Patterson, D. Hah, H. Nguyen, H. Toshiyoshi, R.-m. Chao, and M. C. Wu, "A scanning micromirror with angular comb drive actuation," presented at Fifteenth IEEE International Conference on Micro Electro Mechanical Systems, 20-24 Jan. 2002, Las Vegas, NV, USA, 2002.
38. S. Bourquin, A. D. Aguirre, I. Hartl, P. Hsiung, T. H. Ko, J. G. Fujimoto, T. A. Birks, W. J. Wadsworth, U. Bunting, and D. Kopf, "Ultrahigh resolution real time OCT imaging using a compact femtosecond Nd : Glass laser and nonlinear fiber," Opt. Express **11**, 3290-3297 (2003), http://www.opticsinfobase.org/abstract.cfm?URI=oe-11-24-3290.

1. Introduction

Optical coherence tomography (OCT) is a promising technique for high-resolution *in situ* cross-sectional imaging of biological tissues. Development of scanning fiber-optic catheters has enabled *in vivo* endoscopic OCT imaging [1, 2], and results to date have shown the ability to distinguish tissue architectural layers and to differentiate normal from certain pathologic conditions within the human gastrointestinal tract [3-7]. In recent years, OCT technology has improved significantly. High speed, Fourier domain detection has enabled *in vivo* three-dimensional imaging [8-17], and new technology for *en face* imaging has paved the way for high speed, *in vivo* cellular imaging using optical coherence microscopy [18]. Endoscopic implementation of 3D OCT and OCM imaging, however, requires improvement in catheter device designs. Current endoscopic OCT catheters consist of a single-mode fiber fused to a focusing lens and a microprism to deflect the beam orthogonally away from the fiber axis [1]. These devices are scanned by proximally rotating or translating the fiber. Proximal catheter actuation, however, has poor precision and repeatability and is limited to relatively slow imaging rates due to the physical inertia, friction and compliance of the device. Furthermore, proximal scanning can generally only be performed in one dimension, enabling the generation of a two-dimensional OCT image. For three-dimensional and *en face* imaging applications, new, flexible catheter designs which implement high speed, two-axis scanning at the distal tip of the device are required.

Distal scanning for microscopy applications can be performed either by scanning the fiber tip in the back image plane of the objective or by beam steering using micromirror technologies. Fiber scanning has been performed using piezo-electric devices [19-22] or a balanced tuning fork and lever approach [23]. Micro-electro-mechanical systems (MEMS) mirrors have been demonstrated for beam steering in confocal microscopy [24-28] and in OCT [29-36]. Most fiber scanning approaches require resonant scanning in order to generate sufficient deflection for a reasonable field of view. MEMS mirrors, on the other hand, can perform large angle scanning without resonance, which enables arbitrary scan patterns as well as features such as panning or image rotation. MEMS scanners can also be actuated on resonance to provide high speed raster scanning necessary for *en face* imaging. Furthermore, MEMS devices can operate reliably and with low power consumption, making them suitable for integration into *in vivo* imaging devices.

In this work, a two-dimensional MEMS scanning endoscope was developed and demonstrated for OCT imaging. The MEMS scanning mirror was capable of both DC and

#77304 - $15.00 USD Received 20 November 2006; revised 12 February 2007; accepted 14 February 2007

resonant operation and could produce arbitrary beam scan patterns, enabling cross-sectional, *en face*, and three-dimensional imaging. The integrated endoscope measured approximately 5 mm in diameter and produced a transverse spot size of ~12 μm over an *en face* field of view of 1.8 mm x 1.0 mm. Using the miniaturized probe, ultrahigh resolution two and three-dimensional OCT imaging with < 5 μm axial resolution was demonstrated both *in vivo* and *in vitro*.

2. Catheter design and construction

A scanning electron micrograph of the MEMS optical scanner used in the OCT endoscope is shown in Fig. 1(a). A large 1 mm diameter mirror was driven by angular vertical comb (AVC) actuators, which provided large scan angles for the same comb dimensions compared to standard vertical comb actuators [37]. The comb fingers were self-aligned with a single etching step. The device was realized by combining a foundry surface-micromachining process (MUMPS) with a 3-mask deep-reactive-ion-etching (DRIE) post process. Surface micromachining provides versatile mechanical design and electrical interconnect while bulk micromachining offers flat micromirrors and high-force actuators. The scanner utilized torsion beams and a gimbal-mounting configuration to scan the MEMS mirror in two axes. This design had the advantage of combining the two scan axes to provide a true XY integrated scanner, with a single pivot point. The complete scanner die with the mirror and the actuators measured 3 mm x 3 mm square. Electrical interconnects are shown in Fig. 1(b). To achieve full scanner performance, application of four separate control signals was required, one for each of two sets of comb actuators on both the X and Y axes. Electrostatic actuators have a capacitive load and therefore draw very small amounts of current for low frequency actuations, generally less than 1 to 10 nA.

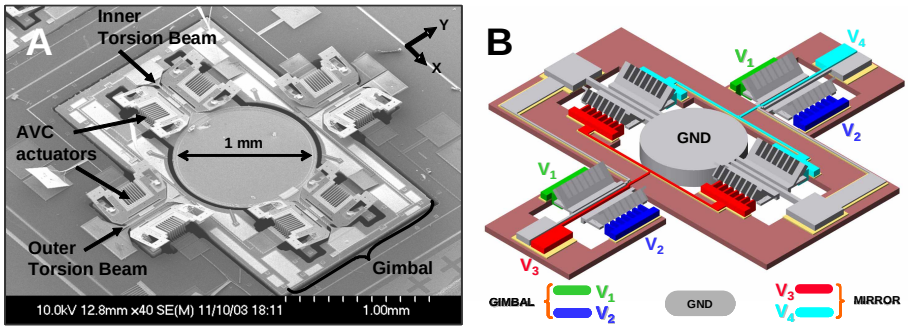

Fig. 1. Scanning electron micrograph (A) and electrical schematic (B) of the MEMS two-axis optical scanner. The scanner has a larger 1 mm diameter mirror and uses angled vertical comb (AVC) actuators to produce a large angle scan for high resolution imaging.

Figure 2 presents the optical and mechanical designs for the MEMS scanning catheter as well as the scanner characteristics measured in the device package. As shown in the optical schematic of Fig. 2(a), light was first collimated to a 1.2 mm diameter beam by a graded-index (GRIN) fiber collimator fused to a single mode optical fiber. A small achromatic lens (f = 10 mm) focused the light onto the specimen. The MEMS optical scanner was mounted at 45 degrees to the optical axis of the lens and redirected the beam out of the endoscope in a similar side-view fashion as used in the conventional OCT catheter [1]. The scanner performed post-objective scanning, which eliminated the off-axis optical aberrations that would be generated if the beam was scanned on the objective lens. Fig. 2(b) provides a mechanical drawing of the catheter package design. The optics and scanner were mounted in a compact aluminum package with a transparent ITO-coated glass window covering the beam

#77304 - $15.00 USD Received 20 November 2006; revised 12 February 2007; accepted 14 February 2007

opening (not shown). The use of the glass window reduced aberration generated by the plastic sheaths used in conventional catheters. The inexpensive outer housing was machined from a single piece of aluminum, which minimized the number of steps required for assembly. The custom package design allowed for precise lateral alignment of the optics using tiny set screws. In addition, the scanner was mounted on an inner carrier block which could be adjusted along the catheter axis to account for lenses with different focal lengths or to set the working distance according to the specific application. The working distance of the catheter used for this study measured ~ 2 mm, and the outermost diameter of the device was ~ 5 mm. This is consistent with confocal scanners which have been integrated into the endoscope head [23] but is larger than the typical accessory working channel in a standard endoscope. Further efforts in the future should lead to reduction of device design below the 3 mm threshold necessary for use in the working channel of an endoscope.

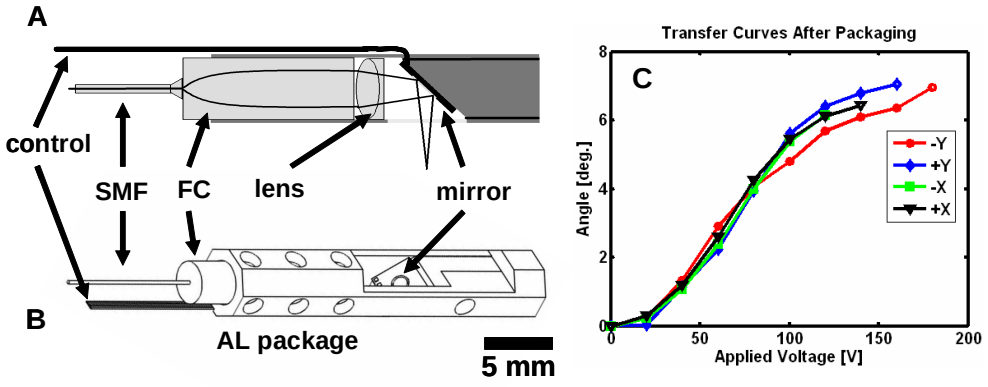

Fig. 2. MEMS catheter design and performance characteristics. (A) Optical schematic. (B) Mechanical drawing. (C) Non-resonant drive characteristics for the MEMS optical scanner after packaging in the catheter endoscope. SMF, single mode fiber. FC, fiber collimator. AL, aluminum.

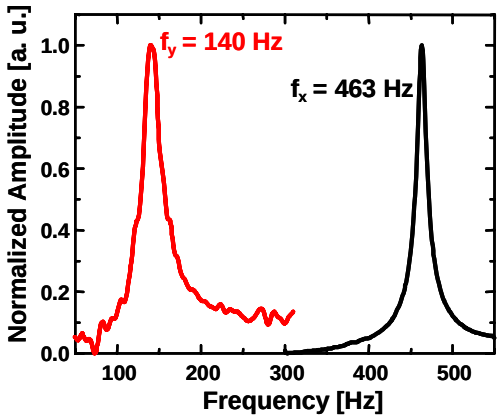

Fig. 3. Resonance characteristics of the MEMS scanner. The mirror resonance was at 463 Hz and the gimbal axis resonance was 140 Hz.

#77304 - $15.00 USD Received 20 November 2006; revised 12 February 2007; accepted 14 February 2007

The non-resonant mechanical scanning angle responses for the four mirror drive controls are presented in Fig. 2(c). It is important to note that these measurements were made with the mirror mounted in the package, which demonstrates the ability of the scanner to function at its optimal performance within an endoscope. Careful attention had to be devoted to bonding issues in mounting the scanner to ensure that device performance was not compromised. The scanner achieved +/- 6 degrees at slightly more than 100 V for both the inner X and outer Y axes. In addition, the optical scanner had excellent frequency response with resonances in the hundreds of Hz for both axes, as shown in Fig 3. Resonant operation of the mirror should enable high-speed raster scanning for *en face* microscopy.

To illustrate the scanner drive control scheme used for imaging, Fig. 4 presents measurements of the position response for the X mirror axis for two different drive waveforms. The position was recorded by detecting an optical beam reflected from the mirror with a two-dimensional position sensor. The response to a triangle drive waveform applied to only one side of the comb actuators is shown in Fig. 4(a). The mirror angle responds as the square of the applied voltage, as shown by the plotted response curve. To compensate for the nonlinear response, a modified drive scheme consisting of a square root function with a DC offset was applied. In addition, the mirror was driven on both axes in a differential manner, which effectively doubled the scan range that could be achieved with a single axis. The resulting angle response had greatly improved linearity, as shown in Fig. 4(b).

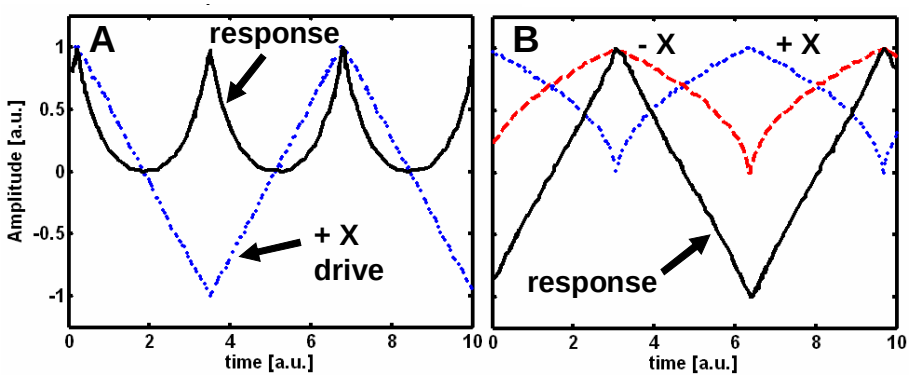

Fig. 4. Drive control scheme for the MEMS optical scanner. (A) Response to a linear drive waveform. (B) Linearized response to a differential, square-root drive function.

3. Two and three-dimensional imaging results

The MEMS OCT endoscope was demonstrated with an ultrahigh resolution OCT imaging system. The system diagram is shown in Fig. 5. The system used a commercially-available femtosecond Nd:glass laser which was spectrally-broadened in a high NA, single mode fiber to a full-width at half-maximum bandwidth of more than 200 nm centered at 1.06 μm [38]. The light source was coupled into a fiber-optic interferometer and split between a reference and a sample arm. Reference delay scanning was performed at ~ 2000 axial scans per second. The MEMS endoscope was placed in the sample arm with an air gap to match the dispersion with the reference arm air path. The interference signal was recorded by a photodetector, and the electronic signal was amplified, filtered, and demodulated before being sampled by a 12-bit, 5 MHz A/D converter and processed by computer. Axial resolution image resolution measured < 4 μm in tissue, while transverse resolution as set by the focusing optics was ~ 12 μm. Imaging was performed with the endoscope at a rate of 4 frames per second over a three-dimensional field of view (X,Y,Z) of 1.8 mm x 1.0 mm x 1.3 mm with 500 x 500 x 1000 pixels.

#77304 - $15.00 USD Received 20 November 2006; revised 12 February 2007; accepted 14 February 2007

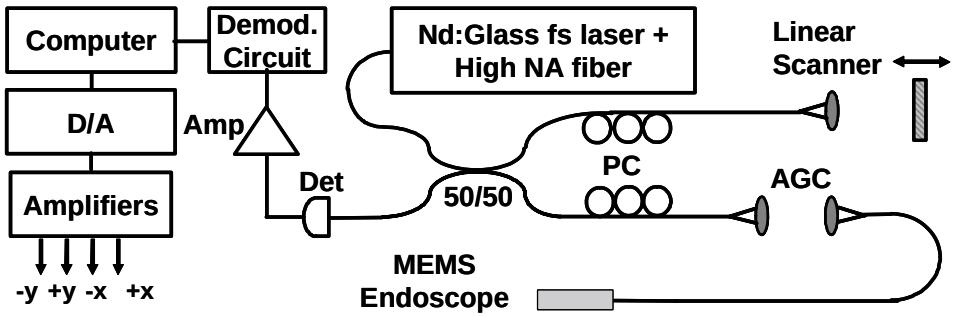

Fig. 5. OCT system schematic for imaging with the MEMS endoscope. PC, polarization control. AGC, air-gap coupling. Det, detector. Amp, amplifier. D/A, digital to analog converter.

Imaging results achieved with the catheter endoscope are presented in Fig. 6. Figures 6(a) and 6(b) present *in vivo* images acquired in human skin. Image quality compares very well with that obtained with the system using a conventional benchtop microscope [38]. Skin from two different locations is shown. A thinner stratum corneum (sc) can be appreciated in Fig. 6(a), which is from the dorsal aspect of the hand, compared to Fig. 6(b), which is from the palmar finger tip. The epidermis and underlying dermis can be seen in both images. Fine structure within the stratum corneum can also be visualized in Fig. 6(b). Figure 6(c) demonstrates an *in vitro* image of lime pulp, used here illustrate the very high axial resolution of the catheter imaging system. Some image stretching at the edges occurs from residual scanner nonlinearity encountered when the rotation angle reverses.

Three-dimensional imaging was performed *in vitro* of hamster cheek pouch with the MEMS scanning catheter endoscope, and representative results are presented in Fig. 6(d) thru 6(f). Volumetric imaging allows visualization of serial two-dimensional sections or reconstruction of a two-dimensional image at an arbitrary image plane, as shown in Fig. 6(d). The volume can also be rendered in three-dimensions to produce a topographical surface representation, illustrated here in Fig. 6(e). To represent the entire data set in a two-dimensional plane, projection techniques can be applied. Figure 6(f) shows an *en face* integrated intensity projection. This view removes the depth dimension, giving a composite perspective which weights structures in depth by scattering intensity. Prominent surface features seen in the projection compare well to those in the rendering. The length of time for acquisition of the 3D volume data set was approximately 2 minutes. These times can be significantly reduced using high speed, Fourier domain OCT techniques.

4. Summary and discussion

A two-axis MEMS scanning catheter with 5 mm outer diameter has been demonstrated for high quality two and three-dimensional ultrahigh resolution OCT imaging. The device produced optical resolution of 12 μm in the transverse dimension and was combined with an OCT system capable of < 4 μm axial resolution in tissue. The scanner had excellent DC response characteristics in packaged form, and a differential drive scheme for linearization of the scanner response was demonstrated for enhanced imaging performance.

#77304 - $15.00 USD Received 20 November 2006; revised 12 February 2007; accepted 14 February 2007

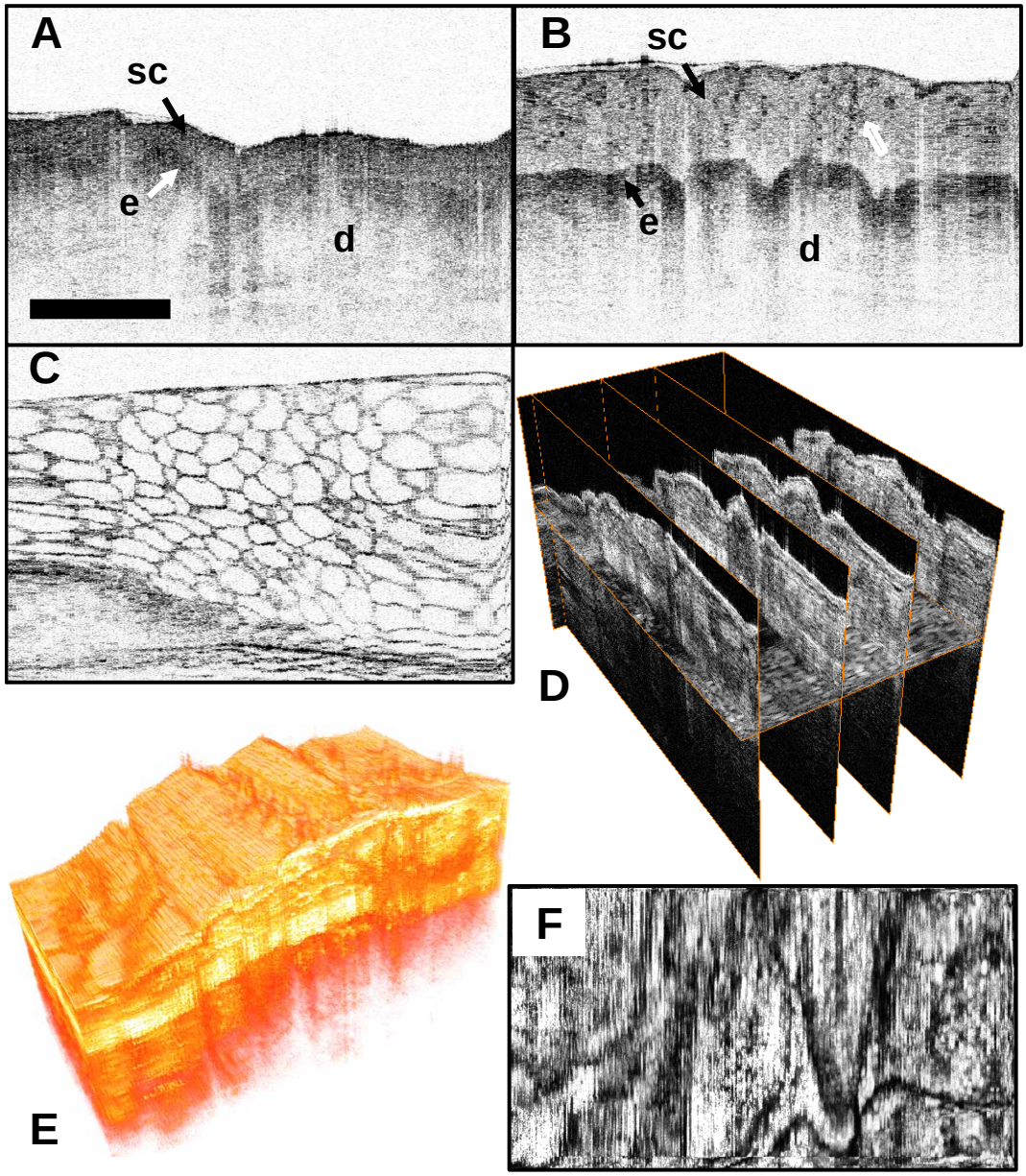

Fig. 6. OCT images acquired with the MEMS scanning catheter. (A,B) *In vivo* cross-sectional images of human skin. sc, stratum corneum; e, epidermis; d, dermis. (C) Cross-sectional image of lime pulp. (D) Serial cross-sections and *en face* plane extracted from a three-dimensional OCT volume of hamster cheek pouch acquired *in vitro*. (E) Three-dimensional rendering of OCT volume data set from the hamster cheek pouch. (F) OCT intensity projection of the 3D volume. Scale bar, 500 μm.

The device design used in this study has several advantages which make it attractive for further development for clinical imaging applications. Post-objective, side-view scanning allows for a simplified optical layout and ease of alignment compared to more complex designs, which require folding of the beam with multiple reflections. Optical aberrations due to pre-objective scanning are eliminated, resulting in improved imaging performance. In

#77304 - $15.00 USD Received 20 November 2006; revised 12 February 2007; accepted 14 February 2007

addition, the inexpensive aluminum package and standard optical components combined with the ability to fabricate the micromirrors in bulk keeps the overall device cost low. Using such designs, it is foreseeable that MEMS based scanning catheters could be disposable if required by the specific application. Finally, the catheter design described here can be made waterproof for future *in vivo* imaging applications by sealing the glass window and the scan head and placing a semi-flexible tubing around the proximal optical fiber and electrical connections. This approach will not increase the outer diameter of the device, which is determined by the dimensions of the scan head.

The MEMS scanner itself had excellent performance characteristics for imaging applications. A 1 mm diameter mirror and good angle response allowed imaging with a large number of resolvable spots. The large mirror aperture would allow for even shorter focal length to reduce transverse spot sizes to < 5 μm. For example, use of a lens with 5 mm focal length can provide a 1/e^2 radius of ~ 3 μm with a working distance from the optical window of several hundred micrometers. For the imaging results presented in this paper, the MEMS scanner was directly driven off resonance with a square-root waveform to produce a linearized response, and DC mechanical angles of +/- 6 degrees were achieved. Response angles of 2-3 times larger will be possible, however, when driving the mirror on resonance. In addition, using bidirectional resonant scanning with scanner responses as shown in Fig. 3, fast image line rates of over 900 Hz and higher should be possible. The fast raster scanning capability combined with tighter focusing optics may enable *en face* optical coherence microscopy for cellular resolution imaging.

The capability for *in vivo* 3D imaging was limited in our study by the relatively slow scan rate of the time-domain OCT system. Future incorporation of these devices with Fourier / spectral domain or swept-source OCT systems will allow much faster 3D imaging [11, 12]. With the advent of very high speed Fourier-domain mode-locked lasers, real-time volumetric imaging at rates of several volumes per second will soon be a reality [17].

In recent years, several groups have made progress toward the development of reliable MEMS based scanners for endoscopic imaging, and a growing body of literature on the subject exists. The task of implementing MEMS-scanning devices for clinical imaging studies remains challenging, however. High speed and linear scanner responses, compact and waterproof device packaging, and development of depth focusing and tissue stabilization schemes are key areas of consideration for future development efforts. Furthermore, the devices presented to date operate in an open-loop mode and lack the precise control that can be achieved with modern galvanometer scanners. Addressing this concern will require increasingly sophisticated scanner technology. Finally, the requirement for relatively high voltages *in vivo* demands a greater level of engineering effort to ensure safety for human studies compared to previous catheter designs, which utilized simple mechanical translation or rotation for scanning. Despite these challenges, development of two-dimensional scanning endoscopes is essential to harness rapid advances in imaging speed and resolution that promise to bring three-dimensional and cellular-level OCT imaging to a clinical reality.

Acknowledgments

A.D. Aguirre and W. Piyawattanametha contributed equally to this work. This research is supported in part by National Science Foundation ECS-0501478 and BES-0522845, National Institutes of Health RO1-CA75289-08 and RO1-EY11289-20, Air Force Office of Scientific Research Medical Free Electron Laser Program FA9550-040-1-0046 and FA9550-040-1-0011, the Poduska Family Foundation Fund for Innovative Research in Cancer, and the philanthropy of Mr. G. Andlinger. A.D. Aguirre acknowledges graduate fellowship support from the Whitaker Foundation and the National Institutes of Health F31-EB00597. W. Piyawattanametha is currently a postdoctoral scholar at Stanford University and L. Fan is currently with Form Factor, Inc.

#77304 - $15.00 USD Received 20 November 2006; revised 12 February 2007; accepted 14 February 2007